Songklanakarin J. Sci. Technol.
46 (2), 209–208, Mar. – Apr. 2024

http://www.sjst.psu.ac.th

Original Article

Design of UVC disinfection system for public transport by optical FEM♣

Suttisak Junarak[1], Eakkachai Warinsiriruk[1*], Promsin Masrinoul[2], Jukrapun Komaikul[2], Phacharakamol Phothisantikul[4], Yin-Tien Wang[3], Kunjimas Ketsuwan[2], and Sanjira Juntarapornchai[2]

[1] *Department of Industrial Engineering, Faculty of Engineering, Mahidol University, Phuttamonthon, Nakhon Pathom, 73170 Thailand*

[2] *Center for Vaccine Development, Institute of Molecular Biosciences, Mahidol University, Phuttamonthon, Nakhon Pathom, 73170, Thailand*

[3] *Department of Mechanical-Electrical Engineering, Tamkang University, Taipei, 25137 Taiwan*

[4] *Brain Storm Engineering and Research Co., Ltd., Bang Khae, Bangkok, 10160 Thailand*

Received: 10 September 2023; Revised: 15 December 2023; Accepted: 7 January 2024

Abstract

The objective of this study was to develop a systematic procedure for implementing Ultraviolet-C (UVC) irradiation in a 21-seat minibus, aiming to improve efficiency of the disinfection system. Utilizing the ANSYS SPEOS® optical design software, a comprehensive 3D simulation of UVC radiation at 280 nm was conducted, covering the passenger seating area. The simulation's objective was to minimize the number of UVC LED lamps needed within the minibus while ensuring a UVC radiation exposure of 15 minutes duration and achieving a log reduction exceeding 1.0 $\log_{10}$ (90%). The simulation determined that a minimum of 9 UVC LED lamps is required for effective disinfection. To validate this simulation-driven approach, Escherichia coli (E. coli) was used to test performance after actual UVC lamp installation. Results from the real-installation disinfection, conducted under optimal parameters, conclusively demonstrated 1.0 $\log_{10}$ (90%) reduction in E. coli and 2.0 $\log_{10}$ (99%) inactivation.

Keywords: UVC irradiance, optical design simulation, cabin, SPEOS®, disinfection efficacy

1. Introduction

Following the Covid-19 pandemic, people are concerned about infections that are airborne or spread by contact (Chow *et al.*, 2023; Morawska & Milton, 2020). Various disinfection methods can be employed to reduce the risk of infection, including chemical methods and UVC irradiation (Jinia *et al.*, 2020; Kwok *et al.*, 2021). Among these alternatives, Ultraviolet-C (UVC) technology exhibits a high disinfection efficacy and has the advantage of not being consumed and having non-thermal operation.

In the present, a variety of light sources has been used at UVC wavelengths, including mercury-vapor UVC lamps at a wavelength of 254 nm, UVC light-emitting diodes (UVC LEDs) at a wavelength of 280 nm, as well as excimer lamps such as krypton chloride excimer (KrCl) at a wavelength of 222 nm (Gerchman *et al.*, 2020; Pereira *et al.*, 2023). Since UVC-LEDs have clear advantages, such as operating without ozone generation (compared to excimer lamps) and being free of mercury (compared to mercury-vapor UVC lamps) (Pereira *et al.*, 2023), this study focused on applying UVC-LEDs at a wavelength of 280 nm in disinfection systems for public transport.

♣Peer-reviewed paper selected from the 10th International Conference on Engineering and Technology
*Corresponding author
Email address: eakkachai.war@mahidol.ac.th

From literature reviews on the disinfection efficacy of UVC-LED light at a wavelength of 280 nm, in the context of SARS-CoV-2, it has been found to achieve efficacious pathogen inactivation by more than 3 log10 (99.9%) under suitable UVC doses of 3.0 mJ/cm² (Cheng *et al.*, 2020).

UVC technology has been implemented for disinfection purposes in areas with high volume of human contact, such as public buildings and mass transit systems (Bertone *et al.*, 2022; Demeersseman *et al.*, 2023). In Thailand, the tourism industry is of paramount importance and relies heavily on public transport. Accordingly, the use of UV radiation for disinfection has become increasingly prominent, replacing traditional chemical-based methods. This approach has found application in public transportation systems across various countries (Drungilas, Kurmis, Tadzijevas, Lukosius, Martinkenas, *et al.*, 2023). In comprehensive reviews of previous research, diverse engineering design strategies have emerged, including the deployment of Robot Disinfection, the Autonomous Mobile Robot (AMR) Disinfection system(Camacho *et al.*, 2021), and simulations aimed at assessing the suitability of integrating UVC technology to enhance disinfection efficacy.

In the field of advanced optical design simulation, such as design of UVC-LEDs irradiation, which is useful in industries for visualized design and analysis of invisible irradiation, the Finite Element Method (FEM) is a powerful tool for virtual analysis (Casado *et al.*, 2017; Ye *et al.*, 2021). Numerous FEM studies have simulated and analyzed UVC-LED irradiation. These methods can determine the irradiance characteristics under pre-processing conditions with idealized assumptions and curve-fitting methods (M. Keshavarzfathy & F. Taghipour, 2019). Some studies assumed a uniform UV irradiation distribution with a specific LED model. The curve-fitting method is useful for specific cases involving meaningful parameters. To estimate the irradiance distribution, the irradiance profile of UVC-LEDs can be represented using curve-fitting. This method assumes a symmetric UV-LED radiation profile that is independent of the azimuthal angle (Majid Keshavarzfathy & Fariborz Taghipour, 2019). Therefore, this procedure is acceptable for use to optimize the pre-processing parameters of an optical simulation for UV irradiation.

This study aimed to establish a systematic procedure for using optical Finite Element Method (FEM) to optimize the installation of UVC-LEDs on a 21-seat minibus. The optimized FEM procedure will be coupled with UVC germicidal data. Additionally, the FEM results will be verified for disinfection efficacy against the pathogens SARs-CoV-2 and E. coli.

2. Materials and Methods

2.1 Light source characteristics

UV ray calculations involve solving the Radiative Transfer Equation (RTE) using various numerical methods, with Monte Carlo and Finite-Volume methods employed commonly. A suggested approach for modeling the radiant energy field of UVC-LEDs considers factors like the actual radiation profile of the UVC-LEDs, media absorption, refraction, reflections at interfaces, and internal surface reflection from the walls. In this method, the RTE is simplified by assuming the insignificance of thermal radiation and scattering, along with a constant absorption coefficient (Majid Keshavarzfathy & Fariborz Taghipour, 2019). Radiometry was employed for irradiance measurement, providing a quantitative evaluation of the radiation model. The close agreement observed between numerical and experimental results highlights the potential of the proposed method for predicting the radiation distribution of UVC-LEDs in a 21-seat minibus. The behavior of photons within an absorbing, scattering, and emitting medium in space is characterized by a Radiative Transfer Equation (RTE). In a steady-state condition for a monochromatic wavelength, the RTE can be formulated as:

$$s \cdot \nabla I(x,s) + (a+\sigma_s) I(x,s) = a I_b(T) + \sigma_s \int_{4\pi} \Phi(s,s') I(x,s') d\Omega(s') \quad (1)$$

where I ($\frac{W}{sr}$) is the radiant intensity, x (m) is the position vector, s is the directional unit vector, a $(\frac{1}{m})$ is the absorption coefficient, σ_s $(\frac{1}{m})$ is the scattering coefficient, I_b $(\frac{W}{sr})$ is the black body emissivity function that depends on the medium temperature (T (K)), Φ is the phase function for the in-scattering of photons, and Ω (sr) is the solid angle about the scattering direction vector s'.

In this paper, the ANSYS SPEOS® module was used to simulate the optical characteristics of UVC-LEDs at wavelength of 280 nm. Figure 2 shows the flow chart of the Finite Element Method (FEM) procedure used to determine the essential parameters of the light source model: Radiant Flux (P), Total Angle (θ_T) and Full Width with Half Maximum in X and Y axis (θ_{Fx}, θ_{Fy}). These parameters directly affect the intensity distribution curve.

In the initial step, a UVC-LED light source from W.I.P ELECTRIC was utilized as the model under study. This light source comprised a 12x1 LED array, providing a resolution of irradiation. Figure 2a shows the micro intensity distribution profile of the light source, and it is assumed to follow a Gaussian distribution due to a silicone lens affecting the emission characteristics. To simulate the LED-UVC intensity in SPEOS®, a surface source with Gaussian distribution is employed, allowing for the adjustment of widespread light emission. The Gaussian distribution exhibits radiant intensity (Figure 2b) and distribution characteristics (Figure 2c). The expression for light intensity can be represented using the formula in Equation 2.

$$I(\theta,\varphi) = exp\left(-\left(\frac{x^2}{2\cdot\sigma_x^2} + \frac{y^2}{2\cdot\sigma_y^2}\right)\right) \quad (2)$$

$$x = \theta \cdot cos\varphi \quad (3)$$

$$y = \theta \cdot sin\varphi \quad (4)$$

$$\sigma_x = \frac{FWHM_x}{2\sqrt{2\cdot ln2}} \quad (5)$$

$$\sigma_y = \frac{FWHM_y}{2\sqrt{2\cdot ln2}} \quad (6)$$

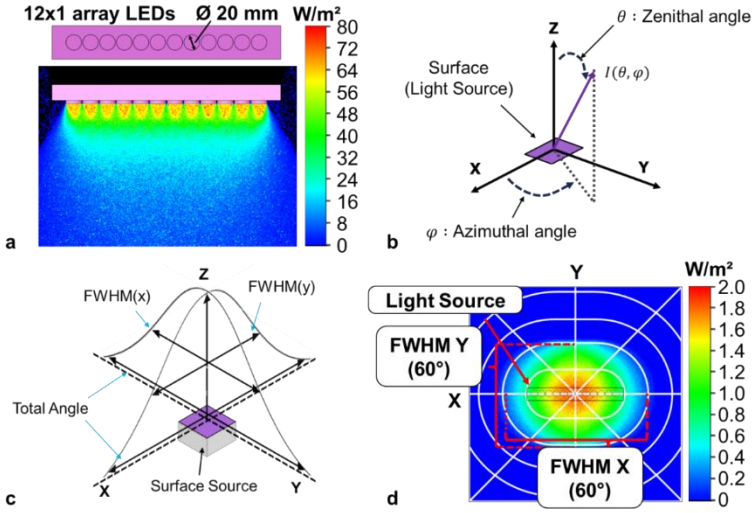

Figure 2. Light source properties: a) The micro-intensity distribution of 12x1 array LEDs module, b) Gaussian distribution notation, c) the asymmetric Gaussian emission profile, and d) the intensity profile of asymmetric Gaussian on surface sensor at total angle 60° and FWHM 60° in both x- and y-directions

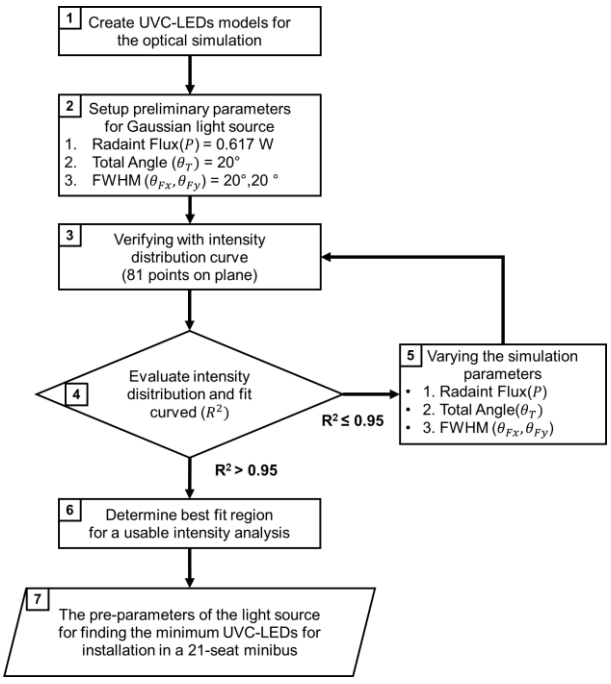

Figure 1. Methodology for defining the light source characteristics of UVC-LED

where $I(\theta, \varphi)$ represents the radiant intensity of surface source, and σ_x and σ_y represent the standard deviations of the Gaussian distribution along the x-axis and the y-axis, respectively.

The second step of the pre-processing simulation is important in this research. Three essential parameters need to be determined through a trial-and-error process using a curve-fitting method. The preliminary input parameters were obtained from the manufacturer's data sheet, as shown in Table 2.

In the third step, the experiment focused on intensity measurement to validate simulation results. The objective was to utilize measurement data for verification. Figure 3a shows a 9 x 9 matrix comprising 81 intensity values arranged on a 1000 x 1000 mm plane (with a resolution of 10x10 mm), depicting a typical intensity distribution curve. For this purpose, a UVC-LED light meter sensor (Linsheng® model 125UV) with a spectral response range of 230 – 315 nm, a resolution of 0.001 W/m², and measuring accuracy of ± 5 μW/cm² was employed. The distance between the light source and the sensor was set at 400 mm, aligning with the actual conditions of the passenger-seat simulation.

Horizontal illuminance, a prevalent method for illuminance calculation, involves integrating light measurements perpendicular to both the horizontal plane and the sensor surface as shown in Figure 3b. Following the Bouguer law, normal illuminance characterizes light intensity changes with the angle of incidence. Radiometry, a reliable technique, is commonly used for measuring irradiance, quantifying radiant flux incident on a specific area. These concepts offer crucial insights into light distribution, applicable in diverse fields, from architecture to environmental science. Horizontal illuminance (E) can be expressed using the formula (Equation 7):

$$E = \frac{I(\theta, \varphi) \cos\theta}{l^2} \quad (7)$$

where E represents the horizontal illuminance, I is the radiant intensity at a specific angle and l is the distance from the light source.

In the fourth step, we will compare the irradiance of simulated data with measured data to assess the pre-parameters, as detailed in the experimental design shown in Figure 4a and utilizing equations 8 and 9. Furthermore, we employ curve-fitting to analyze the data and determine the R-squared value for evaluating the suitability of the parameters. In cases where the simulation results show significant deviation, adjustments will be made to the data to identify parameters that meet the criteria ($R^2 \geq 0.95$).

$$e_{(ij)} = E_{A\,(ij)} - E_{S(ij)} \quad (8)$$

Table 1. Exploring UVC lamp's efficacy and applications of UVC technology

Name			Condition	Results	Highlights
UVC disinfection efficacy	Excimer lamps KrCl (222 nm)	Bacteria E. coli O157:H7 Virus SARS-CoV-2	UVC dose and exposure time dose: 75 mJ/cm² dose: 0.1 mJ/cm² dose: 3 mJ/cm²	 2.81 $\log_{10}$ 0.94 $\log_{10}$ 2.52 $\log_{10}$	- Reduced harm to human skin and eyes - Safety to use - Ozone Generation)Kitagawa *et al.*, 2021; Yin *et al.*, 2015(
	Mercury-vapor UVC (254 nm)	Bacteria E. coli Virus SARS-CoV-2	 dose: 6 mJ/ cm² dose: 1.3 mJ/cm² dose: 10.4 mJ/cm²	 4.00 $\log_{10}$ 1.00 $\log_{10}$ 4.00 $\log_{10}$	- High efficiency - Low cost - Mercury-vapor (Ma *et al.*, 2021; Sesti-Costa *et al.*, 2022)
	LEDs-UVC (255-280 nm)	Virus SARS-CoV-2	 dose: 37.5 mJ/cm² dose: 3.0 mJ/cm² dose: 8.31 mJ/cm²	 3.00 $\log_{10}$ 3.00 $\log_{10}$ 3.00 $\log_{10}$	- No Ozone Production - Application flexibility - High efficiency (Inagaki *et al.*, 2020; Minamikawa *et al.*, 2021; Trivellin *et al.*, 2021)
UVC technology applications	Far-UVC Excimer lamps (222 nm)	A 12 m long M3 city bus	Optimal disinfection is achieved when the far-UVC light source targets the seat with a UVC Dose of 2 mJ/cm²	Disinfection time: - 38.1 min (2 lamps) - 20.6 min (4 lamps) Energy required: - 111.3 Wh (2 lamps) - 109.8 Wh (4 lamps)	- Robotic lamp positioning and lifting/lowering system. - Far-UVC disinfection system installed. - Passenger Detection (Drungilas, Kurmis, Tadzijevas, Lukosius, Sapalas, *et al.*, 2023)
	UVC Lamp (254 nm)	Tests conducted in an enclosed laboratory	Efficient UVC disinfection robot design, path optimization, real-time application prospects.	Improved A-star algorithm with NN sorting: search path length 36.45 m in search time 0.038 sec	- Real-time map-based path planning - Potential applications in various robot domains (Wang *et al.*, 2022)
	UVC-LEDs	Access card reader, bookshelf, and toolbox are in the building	Develop a high-performance disinfection robot with UVC-LEDs for targeted zone disinfection.	E. coli 99% reduction	- High flexibility - Online trajectory planning from integrated interface (Ma *et al.*, 2022)
Simulation analysis for UVC irradiation	UV-LEDs (255 nm)	The difference between model and experimental irradiance values	At a 4 cm distance from LEDs (8 LEDs)	- The variation in the large area is less than 20%. - The small section exhibits a 20-40% variation.	Curve-fitting method (Bowker *et al.*, 2011)
	UV-LEDs (275 nm)		At a 4 cm distance from LEDs (4 LEDs)	- The majority of the variation in the area is less than 10% - Most of the remaining area had under a 20% difference.	
	UV LEDs (260 nm)	Triiodide formation	Flowrate: 109 mL/min; 30 LEDs Flowrate: 109 mL/min; 25 LEDs Flowrate: 190 mL/min; 30 LEDs Flowrate: 190 mL/min; 25 LEDs	1. Difference -8.90% 2. Difference -19.08% 3. Difference 22.83% 4. Difference 15.64%	Drinking water disinfection applications (Jenny *et al.*, 2014)

$$e_{Avg} = \frac{\sum_i \sum_j |e_{(ij)}|}{N} \quad (9)$$

$E_{A\,(ij)}$ and $E_{S(ij)}$ represent the measured data and simulated data, respectively, of UVC-LEDs at position i on the x-axis and j on the y-axis, $e_{(ij)}$ represents the deviation between the measured and simulated irradiance at position indexed by i and j, while e_{avg} represents the average deviation in area indexed by i and j.

In the fifth step, the parameters will be adjusted when the simulated irradiance significantly differs from the measured irradiance. The adjustment will prioritize the intensity at the

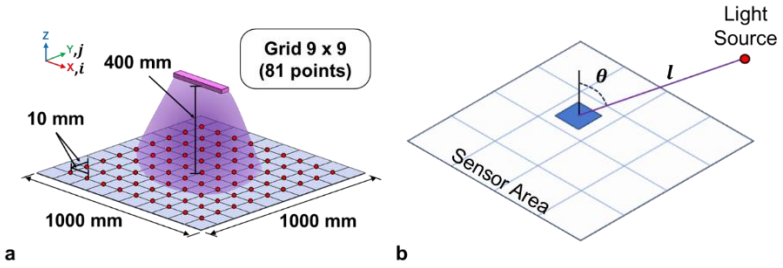

Figure 3. a) Experimental design for measuring UVC-LED module, and b) horizontal illuminance for measuring irradiance

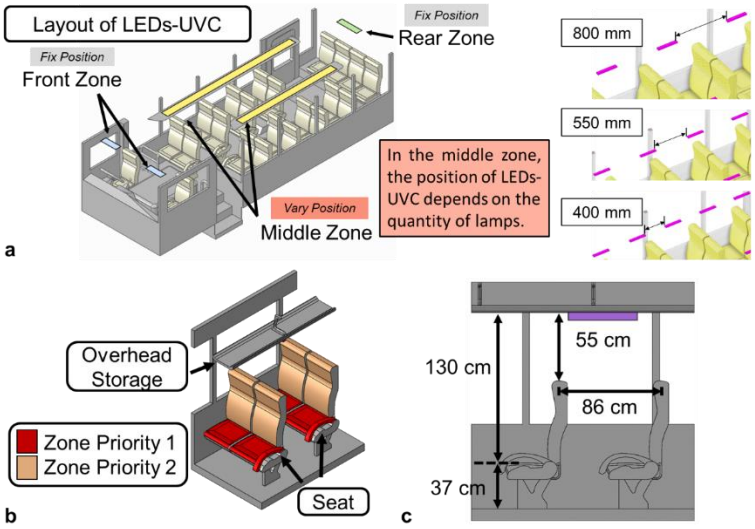

Figure 4. Lighting design simulation in a 21-seat minibus: a) Minibus model for simulation, b) preliminary intensity distribution, and c) preliminary dimensions

Table 2. The preliminary parameters for SPEOS® pre-processing

Parameter	Value
Light source type	Surface type
Material Reflectance	20 %
Irradiance Sensor Type	3D - Irradiance
Radiant Flux(P)	0.617 W
Total Angle (θ_T)	20°
FWHM (θ_{Fx})	20°
FWHM (θ_{Fy})	20°

center of the light source, which has the highest irradiance. Each parameter has specific effects on the simulated irradiance: Power input increases the overall intensity, Total Angle enhances the intensity spread along both the x and y axes but decreases the intensity, and Full Width at Half Maximum affects the shape of the intensity distribution (Equation 10, 11). The simulated intensity is then compared with the measured intensity until it meets the specified criteria.

$$E_{A\,(5,5)} > E_{S(5,5)}; (+)P, (-)\theta_T, (-)\theta_{Fx} \text{ or} (-)\theta_{Fy} \quad (10)$$

$$E_{A\,(5,5)} < E_{S(5,5)}; \ (-)P, (+)\theta_T, (+)\theta_{Fx} \text{ or} (+)\theta_{Fy} \quad (11)$$

In the sixth step, once the pre-parameters obtained from pre-processing meet specific criteria, we will define the usable region. To enhance result accuracy, this region is determined by recognizing that the high-intensity zone efficiently inactivates pathogens, while excluding the low-intensity region to achieve optimal curve fitting for analysis. In the seventh step, we will define the optimal parameters using the pre-parameters obtained from pre-processing within the usable region, following equations 10 and 11. The experimental design details are outlined in Table 3. The objective is to determine setting parameters that have an intensity characteristic similar to the actual features of UVC-LEDs at wavelength of 280 nm. Therefore, this process aims to find the optimal parameters for analyzing the installation layout of UVC-LED lamps on a 21-seat minibus, involving a total of 32 experiments.

2.2 Optimizing light source installation in minibus with 21 seats

In determining the optimal number of light sources for installation on the 21-seat minibus, our initial step involves creating a model of the minibus, using the dimensions of a typical minibus employed. The case study design, outlined in Figure 4a, investigates UVC-LED intensity on the minibus, divided into three sections: the front zone, middle zone, and rear zone. Fixed positions for the front and rear zones include two lamps installed above the driver and passenger seats, and one lamp in the middle of the rear seat row. We will explore three scenarios, each with lamps placed along the longer length of the minibus: 9 lamps, 11 lamps, and 13 lamps.

Table 3. Light source parameters and levels

Parameter	Level-1	Level-2	Level-3
Power input: Radiant flux (W)	0.2	0.22	-
Total angle (θ_T)	65	70	-
FWHM in X (θ_{Fx})	50	55	60
FWHM in Y (θ_{Fy})	55	60	65

Meshing strategically optimizes computational resources by targeting specific geometric regions, thereby enhancing result granularity through the subdivision of the model into manageable blocks, typically triangular shaped, within CAD software. This focused computational approach is particularly beneficial in simulations where the interpretation of incoming rays involves numerous intricately meshed components.

In the evaluation of LED-UVC irradiance within a 21-seat minibus, the essential requirement is the incorporation of a 3D irradiance sensor. To compute the 3D irradiation, internal objects within the minibus must be converted by using the Facet function in ANSYS SPEOS®, with the Max edge length parameter set to 2 mm. This specific configuration aims for high detail, allowing for a reduction in the maximum edge length to enhance mesh surface intricacy.

As a preliminary step, we'll prioritize seats in zones based on the volume of human contact. Priority zone 1 has the highest human contact volume, while priority zone 2 comes next (Figure 4b). Figure 4c shows the dimensions of the preliminary model, and we aim to simulate the intensity on seats for determining the installation positions of lamps. The goal is to minimize the number of UVC lamps in the 21-seat minibus while achieving a sufficient UVC dose to inactivate the pathogen within a 30-minute exposure time.

The disinfection efficacy was evaluated through logPFU ratio following equation 12. The infectious titer reduction rate followed equation 13 (Inagaki *et al.*, 2020).

$$\text{logPFU} = \log_{10}\left(\frac{N_t}{N_0}\right) \qquad \text{logPFU} = \log_{10}\left(\frac{N_t}{N_0}\right) \tag{12}$$

$$\text{activate reduction} = \left(1 - \frac{1}{10^{\log \text{PFU}}}\right) \text{x } 100 \tag{13}$$

where N_t is PFU count after exposure by UV-irradiance and N_0 is initial PFU count.

3. Results and Discussion

3.1 Results of lights source characteristic analysis

In the pre-processing study, optimal pre-parameters were power input 0.2W, total angle 70°, FWHM 55°, and 60° in x and y respectively**.** The high irradiance usable region was between 30 **-** 70cm in X and Y axes (Figure 5a and 5b). Deviation occurred in low irradiance outside the Confidence Interval, but R^2 met its criteria ($R^2 > 0.95$) (Figure 5c). For accuracy, focus was on usable region due for the best curve fitting at high irradiance. Most values fell within the specified range (95% Confidence Interval) (Greenland, 2004), with an R^2 value of 0.977 (Figure 5d).

After defining the usable region on a plane, the UV irradiance will be analyzed within this boundary (Figure 6). In the parameter study, it is observed that the center of the plane commonly exhibits the highest UV irradiance, with a continuous decrease depending on the Full Width at Half Maximum (FWHM) of each axis**.** The result shows the average deviation of comparison data ranged from 7.65% to 16.01%. The optimal parameters with the lowest average deviation are Power Input, Total Angle, and FWHM in X and Y axes, set at 0.2 Watt, 65°, 50°, and 60°, respectively, as shown in Figure 7. These parameters will be applied to simulate the light distribution of LED-UVC inside a 21-seat minibus.

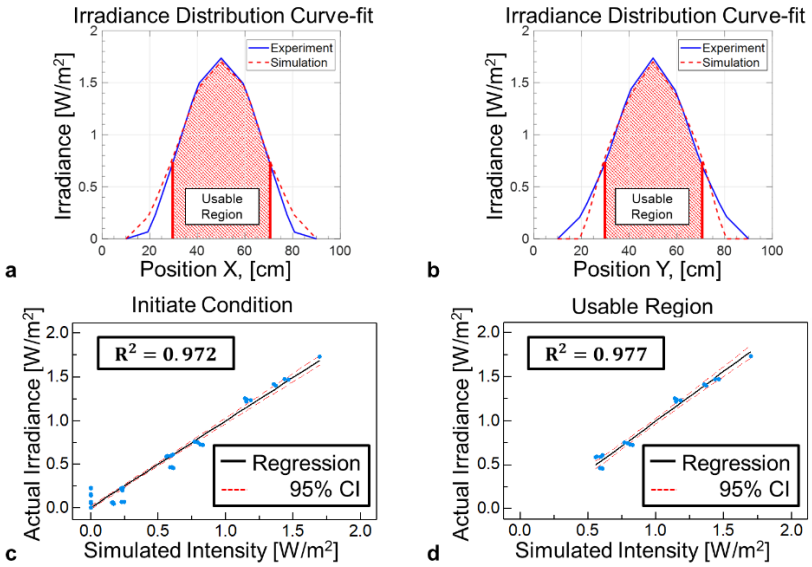

Figure 5. Comparison of actual and simulation results. a) Irradiance curve-fit in x-axis, b) irradiance curve-fit in y-axis, c) regression of irradiance comparison on plane (81 points), and d) regression of irradiance comparison on usable region (21 points)

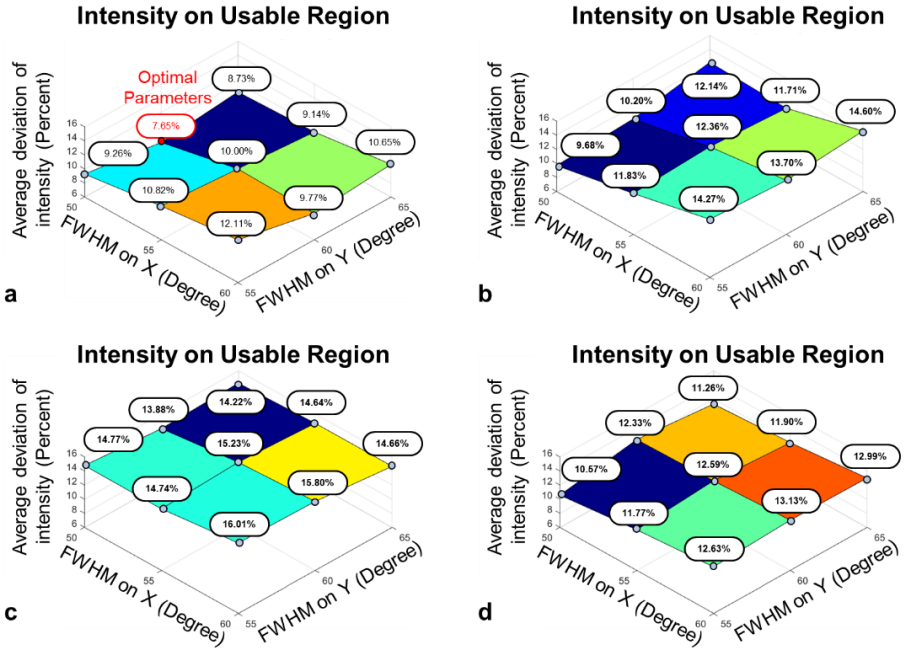

Figure 7. The average spread on usable region for a) P = 0.2 watt, $\theta_T = 65°$, b) P = 0.2 watt, $\theta_T = 70°$, c) P = 0.22 watt, $\theta_T = 65°$, and d) P = 0.22 watt, $\theta_T = 70°$

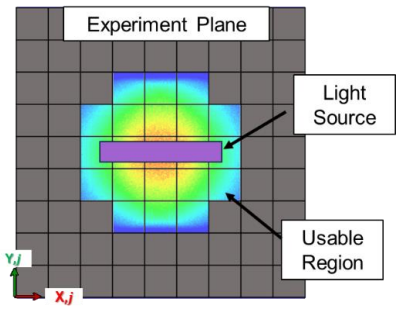

Figure 6. Light irradiance on plane in usable region

3.2 Results of intensity distribution on minibus with 21 seats

In the initial intensity distribution (Figure 8a), seat pads and armrests show UV intensity between 0.20 - 0.40 W/m², back seats and headrests range from 0.10 - 0.30 W/m², and 0.10 - 0.90 W/m², respectively, in the UV irradiance on priority zone 1 (seat pad and armrest) within a 21-seat minibus across scenarios. In Scenario 1, the average irradiance is 0.139 W/m², ranging from 0.103 W/m² to 0.166 W/m² (Figure 8b). For Scenario 2, the average irradiance is 0.177 W/m², with values ranging from 0.170 W/m² to 0.185 W/m² (Figure 8c). In Scenario 3, the average irradiance is 0.220 W/m², with a range from 0.103 W/m² to 0.166 W/m² (Figure 8d).

In the analysis of disinfection scenarios for E. coli, achieving a 3 log10 (99.9%) reduction requires minimum irradiation durations of 859, 673, and 541 seconds, reaching a UV dose of 119 J/m² (Cheng *et al.*, 2020). For SARS-CoV-2, a 3 log10 (99.9%) reduction demands minimum irradiation durations of 217, 170, and 136 seconds, reaching a UV dose of 30 J/m² (Minamikawa *et al.*, 2021) in scenarios with 9 lamps, 11 lamps, and 13 lamps, respectively (Figure 9).

Concerning a cost analysis, UVC-LEDs at a wavelength of 280 nm cost approximately 10,000 THB per lamp. So, for each scenario, the investment cost is 90,000, 110,000, and 130,000 THB, respectively, excluding modification and installation costs.

The disinfection efficacy target is to inactivate bacteria and viruses on the minibus surface within 15 minutes. Therefore, based on simulation results, choosing 9 UVC-LED lamps is sufficient for pathogen reduction by more than 90% (D90). Additionally, if we aim to reduce the disinfection cost while maintaining a high efficacy target, Scenario 1 with 9 lamps appears to be a cost-effective choice due to its lower investment cost of 90,000 THB compared to 110,000 THB for Scenario 2 and 130,000 THB for Scenario 3,

To validate the installation layout of UVC-LEDs at wavelengths of 280 nm in scenario 1 for sufficient surface irradiance in disinfection, E. coli bacteria will be employed. Since the high biosafety hazard associated with SARS-CoV-2 and the requirement for specialized equipment, testing for SARS-CoV-2 will be conducted in a laboratory to validate disinfection efficacy. Samples of E. coli will be strategically placed inside the minibus at various irradiance intensities as shown in Figure 8.

The results are shown in Table 5. With irradiation for 15 minutes, the UV dose reached 125 J/m², and inactivated E. Coli by more than 4.00 $\log_{10}$ (99.99%) in 7 of 10 positions in the minibus. With irradiation for 30 minutes, the UV dose reached 250 J/m², and inactivated E. Coli by more than 4.00 $\log_{10}$ (>99.99%) in 9 of 10 positions in the minibus. The lowest inactivation was 96.50% on the back-row passenger seat pad. Overall, in all positions prioritized in the bus, pathogen inactivation was by more than 1.00 $\log_{10}$ (90%).

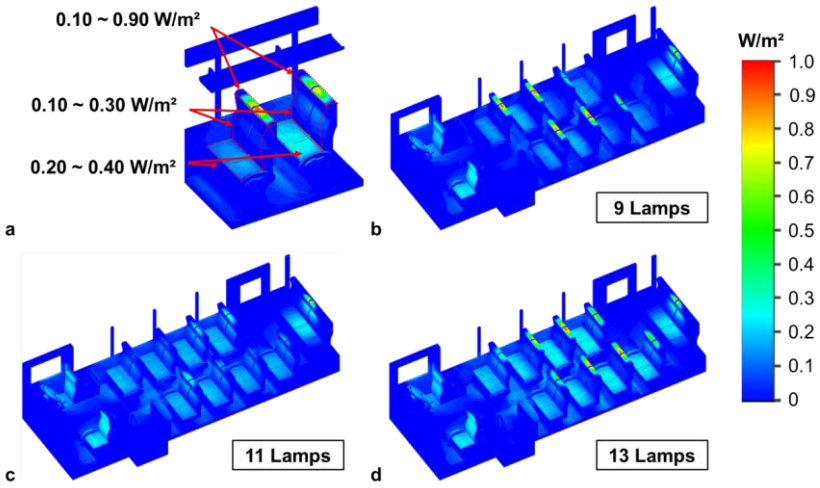

Figure 8. The intensity distribution from simulation: a) preliminary on 2 seats, b) 9 lamps in minibus, c) 11 lamps in minibus, and d) 13 lamps in minibus

Table 4. Light source parameters and experimental results

No.	Radiant flux (W)	Total angle (°)	$FWHM_X$ (°)	$FWHM_Y$ (°)	e_{Avg}
1	0.20	65	50	55	9.26%
2	0.20	65	50	60	7.65%
3	0.20	65	50	65	8.73%
4	0.20	65	55	55	10.82%
5	0.20	65	55	60	10.00%
6	0.20	65	55	65	9.14%
7	0.20	65	60	55	12.11%
8	0.20	65	60	60	9.77%
9	0.20	65	60	65	10.65%
10	0.20	70	50	55	9.68%
11	0.20	70	50	60	10.20%
12	0.20	70	50	65	12.14%
13	0.20	70	55	55	11.83%
14	0.20	70	55	60	12.36%
15	0.20	70	55	65	11.71%
16	0.20	70	60	55	14.27%
17	0.20	70	60	60	13.70%
18	0.20	70	60	65	14.60%
19	0.22	65	50	55	14.77%
20	0.22	65	50	60	13.88%
21	0.22	65	50	65	14.22%
22	0.22	65	55	55	14.74%
23	0.22	65	55	60	15.23%
24	0.22	65	55	65	14.64%
25	0.22	65	60	55	16.01%
26	0.22	65	60	60	15.80%
27	0.22	65	60	65	14.66%
28	0.22	70	50	55	10.57%
29	0.22	70	50	60	12.33%
30	0.22	70	50	65	11.26%
31	0.22	70	55	55	11.77%
32	0.22	70	55	60	12.59%
33	0.22	70	55	65	11.90%
34	0.22	70	60	55	12.63%
35	0.22	70	60	60	13.13%
36	0.22	70	60	65	12.99%

Table 5. The disinfection of E. Coli bacteria by UVC-LEDs at 280 nm over 15-minute and 30-minute durations

Time of exposure (minutes)	No.	Sample Code	Antivirus activation		
			CFU/ml	Log reduction	% Reduction
15 (UV dose 125 J/m²)	1	Position 1	1,300	5.30	> 99.9%
	2	Position 2	1,500	5.24	> 99.9%
	3	Position 3	8	7.51	> 99.9%
	4	Position 4	1,500	5.24	> 99.9%
	5	Position 5	1,900,000	2.14	99.27%
	6	Position 6	240	6.03	> 99.9%
	7	Position 7	1,000,000	2.42	99.62%
	8	Position 8	9,100,000	1.46	96.50%
	9	Position 9	260	6.00	> 99.9%
	10	Position 10	240	6.04	> 99.9%
30 (UV dose 250 J/m²)	1	Position 1	1,200	5.34	> 99.9%
	2	Position 2	1,300	5.30	> 99.9%
	3	Position 3	3	7.94	> 99.9%
	4	Position 4	15	7.24	> 99.9%
	5	Position 5	1,500	5.24	> 99.9%
	6	Position 6	1,600	5.21	> 99.9%
	7	Position 7	1,900	5.14	> 99.9%
	8	Position 8	4,600,000	1.75	98.23%
	9	Position 9	190	6.14	> 99.9%
	10	Position 10	170	6.19	> 99.9%

Positive Control at 15 min is 260,000,000 (2.6E+08)

For the SARS-CoV-2 virus, the UVC-LED lamp was positioned 15 cm above the SARS-CoV-2 plate. The inactivation results are summarized in Table 6. Achieving a UV dose of 50 J/m² in 8 seconds resulted in a disinfection efficacy of 2.84 $\log_{10}$ (99.86%). A UV dose of 100 J/m² was reached in 16 seconds, ensuring a disinfection efficacy by more than 4.00 $\log_{10}$ (99.99%).

Table 6. The efficacy of SARS-CoV-2 virus disinfection in a laboratory by UVC-LEDs at 280 nm

UVC device	UVC dose target (J/m^2)	Time of exposure (seconds)	Virus titer (pfu/mL)	Antivirus activation	
				Log reduction	% Reduction
LEDs-UVC (280 nm)	50	8	$4.33 \times 10^3 \pm 3.28 \times 10^3$	2.84	99.86
	100	16	$< 10^2$	≥ 4.4	≥ 99.99*
Untreated (Control)	-	1785.7 ($\approx$ 29.8 min)	$2.25 \times 10^6 \pm 1.15 \times 10^5$	-	-

*Virus was not detected at the limit of detection

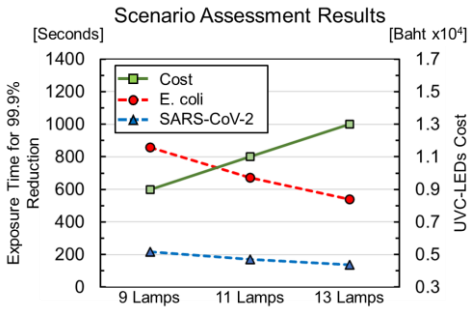

Figure 9. Cost and minimum exposure time analysis for 99.9% inactivation of SARS-CoV-2 and E. Coli in each scenario

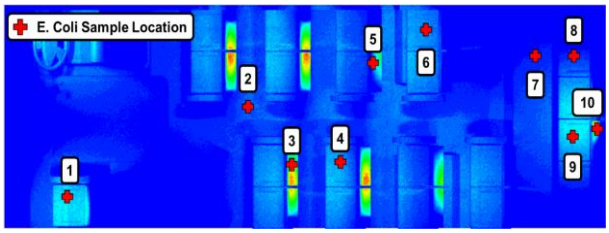

Figure 10. Schematic of scenario validation using Escherichia coli

4. Conclusions

We identified Scenario 1, utilizing 9 lamps, as the most effective configuration for the public transport disinfection system. This setup demonstrated inactivation efficacy against E. coli and SARS-CoV-2, achieving a 3 log10 (99.9%) reduction within a 15-minute exposure. This decision is grounded on a careful balance between disinfection efficacy and cost considerations.

To ensure the practical effectiveness of the disinfection system, we validated the inactivation efficacies against E. coli and SARS-CoV-2. The minimum inactivation efficacy observed for E. coli was 1.46 log10 (96.5%) at a UV dose of 125 J/m^2, and for SARS-CoV-2, it was 2.84 log10 (99.86%) at a UV dose of 50 J/m^2. This thorough approach gives confidence in the proposed disinfection system to establish a safe and pathogen-free environment in public transport.

Acknowledgements

This research was supported by Thailand' PMU-C in the future motility sector.

References

Bertone, M., Mikszewski, A., Stabile, L., Riccio, G., Cortellessa, G., d'Ambrosio, F. R., . . . Buonanno, G. (2022). Assessment of SARS-CoV-2 airborne infection transmission risk in public buses. *Geoscience Frontiers*, *13*(6), 101398. Retrieved from https://doi.org/10.1016/j.gsf.2022.101398

Bowker, C., Sain, A., Shatalov, M., & Ducoste, J. (2011). Microbial UV fluence-response assessment using a novel UV-LED collimated beam system. *Water Research*, *45*(5), 2011-2019. Retrieved from https://doi.org/10.1016/j.watres.2010.12.005

Camacho, E. C., Ospina, N. I., & Calderón, J. M. (2021). COVID-Bot: UV-C based autonomous sanitizing robotic platform for COVID-19. *IFAC-Papers OnLine*, *54*(13), 317-322. Retrieved from https://doi.org/https://doi.org/10.1016/j.ifacol.2021.10.466

Casado, C., Timmers, R., Sergejevs, A., Clarke, C. T., Allsopp, D. W. E., Bowen, C. R., . . . Marugán, J. (2017). Design and validation of a LED-based high intensity photocatalytic reactor for quantifying activity measurements. *Chemical Engineering Journal*, *327*, 1043-1055. Retrieved from https://doi.org/10.1016/j.cej.2017.06.167

Cheng, Y., Chen, H., Sanchez Basurto, L. A., Protasenko, V. V., Bharadwaj, S., Islam, M., & Moraru, C. I. (2020). Inactivation of Listeria and E. coli by deep-UV LED: Effect of substrate conditions on inactivation kinetics. *Scientific Reports*, *10*(1), 3411. Retrieved from https://doi.org/10.1038/s41598-020-60459-8

Chow, E. J., Uyeki, T. M., & Chu, H. Y. (2023). The effects of the COVID-19 pandemic on community respiratory virus activity. *Nature Reviews Microbiology*, *21*(3), 195-210. Retrieved from https://doi.org/10.1038/s41579-022-00807-9

Demeersseman, N., Saegeman, V., Cossey, V., Devriese, H., & Schuermans, A. (2023). Shedding a light on ultraviolet-C technologies in the hospital environment. *Journal of Hospital Infection*, *132*, 85-92. Retrieved from https://doi.org/10.1016/j.jhin.2022.12.009

Drungilas, D., Kurmis, M., Tadzijevas, A., Lukosius, Z., Martinkenas, A., Didziokas, R., . . . Jankunas, V. (2023). Evaluating the impact of 222 nm far-UVC radiation on the aesthetic and mechanical properties of materials used in public bus interiors. *Applied Sciences*, *13*(7). Retrieved from https://doi.org/10.3390/app13074141

Drungilas, D., Kurmis, M., Tadzijevas, A., Lukosius, Z., Sapalas, D., Jankunas, V., . . . Gruode, J. (2023). Development of far-UVC-based surface disinfection prototype for public buses. *Applied Sciences*, *13*(14). Retrieved from https://doi.org/10.3390/app13148501

Gerchman, Y., Mamane, H., Friedman, N., & Mandelboim, M. (2020). UV-LED disinfection of Coronavirus: Wavelength effect. *Journal of Photochemistry and Photobiology B: Biology*, *212*, 112044. Retrieved from https://doi.org/https://doi.org/10.1016/j.jphotobiol.2020.112044

Greenland, S. (2004). Interval estimation by simulation as an alternative to and extension of confidence intervals. *International Journal of Epidemiology*, *33*(6), 1389-1397. Retrieved from https://doi.org/10.1093/ije/dyh276

Inagaki, H., Saito, A., Sugiyama, H., Okabayashi, T., & Fujimoto, S. (2020). Rapid inactivation of SARS-CoV-2 with deep-UV LED irradiation. *Emerging Microbes and Infections*, *9*(1), 1744-1747. Retrieved from https://doi.org/10.1080/22221751.2020.1796529

Jenny, R. M., Simmons, O. D., Shatalov, M., & Ducoste, J. J. (2014). Modeling a continuous flow ultraviolet Light Emitting Diode reactor using computational fluid dynamics. *Chemical Engineering Science*, *116*, 524-535. Retrieved from https://doi.org/10.1016/j.ces.2014.05.020

Jinia, A. J., Sunbul, N. B., Meert, C. A., Miller, C. A., Clarke, S. D., Kearfott, K. J., . . . Pozzi, S. A. (2020). Review of sterilization techniques for medical and personal protective equipment contaminated with SARS-CoV-2. *IEEE Access*, *8*, 111347-111354. Retrieved from https://doi.org/10.1109/ACCESS.2020.3002886

Keshavarzfathy, M., & Taghipour, F. (2019). Computational modeling of ultraviolet light-emitting diode (UV-LED) reactor for water treatment. *Water Research*, *166*, 115022. Retrieved from https://doi.org/10.1016/j.watres.2019.115022

Keshavarzfathy, M., & Taghipour, F. (2019). Radiation modeling of ultraviolet light-emitting diode (UV-LED) for water treatment. *Journal of Photochemistry and Photobiology A: Chemistry*, *377*, 58-66. Retrieved from https://doi.org/10.1016/j.jphotochem.2019.03.030

Kitagawa, H., Nomura, T., Nazmul, T., Omori, K., Shigemoto, N., Sakaguchi, T., & Ohge, H. (2021). Effectiveness of 222-nm ultraviolet light on disinfecting SARS-CoV-2 surface contamination. *American Journal of Infection Control*, *49*(3), 299-301. Retrieved from https://doi.org/10.1016/j.ajic.2020.08.022

Kwok, C. S., Dashti, M., Tafuro, J., Nasiri, M., Muntean, E.-A., Wong, N., . . . Mallen, C. D. (2021). Methods to disinfect and decontaminate SARS-CoV-2: a systematic review of in vitro studies. *Therapeutic Advances in Infectious Disease*, *8*, 20499361219985548. Retrieved from https://doi.org/10.1177/2049936121998548

Ma, B., Gundy, P. M., Gerba, C. P., Sobsey, M. D., & Linden, K. G. (2021). UV Inactivation of SARS-CoV-2 across the UVC spectrum: KrCl* excimer, mercury-vapor, and light-emitting-diode (LED) sources. *Applied and Environmental Microbiology Journal*, *87*(22), e0153221. Retrieved from https://doi.org/10.1128/AEM.01532-21

Ma, Y., Xi, N., Xue, Y., Wang, S., Wang, Q., & Gu, Y. (2022). Development of a UVC-based disinfection robot. *Industrial Robot: the international journal of robotics research and application*, *49*(5), 913-923. Retrieved from https://doi.org/10.1108/ir-10-2021-0227

Minamikawa, T., Koma, T., Suzuki, A., Mizuno, T., Nagamatsu, K., Arimochi, H., . . . Nomaguchi, M. (2021). Quantitative evaluation of SARS-CoV-2 inactivation using a deep ultraviolet light-emitting diode. *Scientific Reports*, *11*(1), 5070. Retrieved from https://doi.org/10.1038/s41598-021-84592-0

Morawska, L., & Milton, D. K. (2020). It is time to address airborne transmission of coronavirus disease 2019 (COVID-19). *Clinical Infectious Diseases*, *71*(9), 2311-2313. Retrieved from https://doi.org/10.1093/cid/ciaa939

Pereira, A. R., Braga, D. F. O., Vassal, M., Gomes, I. B., & Simões, M. (2023). Ultraviolet C irradiation: A promising approach for the disinfection of public spaces? *Science of The Total Environment*, *879*, 163007. Retrieved from https://doi.org/10.1016/j.scitotenv.2023.163007

Sesti-Costa, R., Negrao, C. V. Z., Shimizu, J. F., Nagai, A., Tavares, R. S. N., Adamoski, D., . . . Dias, S. M. G. (2022). UV 254 nm is more efficient than UV 222 nm in inactivating SARS-CoV-2 present in human saliva. *Photodiagnosis and Photodynamic Therapy*, *39*, 103015. Retrieved from https://doi.org/10.1016/j.pdpdt.2022.103015

Trivellin, N., Buffolo, M., Onelia, F., Pizzolato, A., Barbato, M., Orlandi, V. T., . . . Meneghini, M. (2021). Inactivating SARS-CoV-2 using 275 nm UV-C LEDs through a spherical irradiation box: Design, Characterization and Validation. *Materials (Basel)*, *14*(9). Retrieved from https://doi.org/10.3390/ma14092315

Wang, S., Li, Y., Ding, G., Li, C., Zhao, Q., Sun, B., & Song, Q. (2022). Design of UVC surface disinfection robot with coverage path planning using map-based approach at-the-edge. *Robotics*, *11*(6). Retrieved from https://doi.org/10.3390/robotics11060117

Ye, Z. T., Cheng, Y. H., Hung, L. W., Hsu, K. H., & Hu, Y. C. (2021). Light guide layer thickness optimization for enhancement of the light extraction efficiency of ultraviolet light-emitting diodes. *Nanoscale Research Letters*, *16*(1), 106. https://doi.org/10.1186/s11671-021-03563-6

Yin, F., Zhu, Y., Koutchma, T., & Gong, J. (2015). Inactivation and potential reactivation of pathogenic Escherichia coli O157:H7 in apple juice following ultraviolet light exposure at three monochromatic wavelengths. *Food Microbiology*, *46*, 329-335. Retrieved from https://doi.org/10.1016/j.fm.2014.08.015